University of Crete

Master Thesis

Gamma-Rays from the high-redshift Universe

Author:
Ioannis Komis

Supervisor:
Vasiliki Pavlidou
Co-Supervisor:
Andreas Zezas

A thesis submitted in fulfilment of the requirements
for the degree of Masters of Science
in the Faculty of Physics

Physics Department
Greece
June 2016

"It doesn't matter how beautiful your theory is,
it doesn't matter how smart you are,
if it doesn't agree with experiment,
it's wrong!

Richard P. Feynman

Gamma-Rays from the high-redshift Universe

Ioannis Komis

Abstract

The present thesis is a study of gamma-rays from the high-redshift Universe. In particular, we examine normal star-forming galaxies as one of the main components of the extragalactic gamma-ray background (EGRB). Despite the new data from the Fermi Gamma-Ray Space Telescope that have been collected through the eight years of operation, the contribution of normal star-forming galaxies to the extragalactic gamma-ray background (EGRB) remains poorly constrained. In this work, we present a comprehensive analysis of factors that can affect estimates of the EGRB: a) possible sources of redshift dependence of the gamma-ray emissivity of a typical galaxy including evolving metallicity, b) cosmic star-formation history and c) the slope of the scaling between star formation tracers and gamma-ray luminosity. Since the number of resolved galaxies is small (8 galaxies), we explicitly test the effect of small number statistics to the empirical slope of this scaling. We conclude that the results are sensitive to the number of resolved galaxies, and we place upper and lower limits to the potential contribution of star forming galaxies to the EGRB for energies between 100 MeV and 100 GeV.

Ακτινοβολία-γ από περιοχές του σύμπαντος με υψηλή ερυθρόπηση

Ιωάννης Κόμης

Περίληψη

Η παρούσα εργασία είναι μια μελέτη της ακτινοβολίας-γ από περιοχές του σύμπαντος με υψηλή ερυθρόπηση. Συγκεκριμένα, εξετάζουμε τους γαλαξίες με ομαλή αστρική γένεση ως ένα από τα κύρια συστατικά του εξωγαλαξιακού υποβάθρου ακτινοβολίας-γ. Παρά τα νέα δεδομένα από το διαστημικό τηλεσκόπιο ακτίνων-γ Fermi, τα οποία συλλέχθηκαν μετά από οκτώ χρόνια λειτουργίας, η συμβολή των παραπάνω γαλαξιών στο εξωγαλαξιακό υπόβαθρο ακτινοβολίας-γ παραμένει αβέβαιη. Σε αυτή την εργασία, παρουσιάζουμε μια ολοκληρωμένη ανάλυση των παραγόντων που μπορούν να επηρεάσουν τις εκτιμήσεις του εξωγαλαξιακού υποβάθρου ακτινοβολίας-γ: α) πιθανή εξάρτηση από την ερυθρόπηση της εκπομπής ακτινοβολίας-γ από ένα τυπικό γαλαξία συμπεριλαμβανομένης και την εξέλιξη της μεταλλικότητας, β) η κοσμική ιστορία της αστρικής γένεσης γ) κλίση της εξάρτησης της φωτεινότητας σε ακτίνες-γ από ποσότητες που υποδεικνύουν το ρυθμό αστρικής γένεσης. Δεδομένου οτι ο αριθμός των ανιχνευθέντων γαλαξιών είναι μικρός (8 γαλαξίες), εξετάζουμε εκπεφρασμένα την επίδραση του μικρού μεγέθους του στατιστικού δείγματος στην εμπειρική κλίση της παραπάνω εξάρτησης. Καταλήγουμε στο συμπέρασμα οτι τα αποτελέσματα μας είναι ευαίσθητα στον αριθμό ανιχνευθέντων γαλαξιών και θέτουμε πάνω και κάτω όρια στην πιθανή συνεισφορά των γαλαξιών με αστρογένεση στο εξωγαλαξιακό υπόβαθρο ακτινοβολίας-γ για ενέργειες από 100 MeV έως 100 GeV.

Acknowledgements

Firstly, I would like to thank my supervisors Vasiliki Pavlidou and Andreas Zezas for their guidance, patient and support. Professor Pavlidou, with her enthusiasm and optimism, has a unique way to encourage you so that you overcome every obstacle. Her advice not only for this work but also for my upcoming career as a researcher were extremely important. Professor Zezas, with his immense knowledge, helped me through our meaningful discussions complete this work.

I would also like to express my sincere gratitude to my parents for their support through the years. Without them I would not be able to reach my goals and keep trying to accomplish even more. For these reasons I dedicate this thesis to them.

Last but not least, I thank my friends for their help and the great discussions we had. With Aris Tritsis, Kostas Mouloudakis, Panagiotou Christos and Sophie Tsiatsiou we had a wonderful time in the University of Crete all these years. Aris had also helped me learning Python which was crucial for the fulfilment of this work.

To my family

Contents

Chapter 1

Introduction

The gamma-ray sky consists of resolved point sources, galactic diffuse emission, i.e., cosmic rays interaction with the interstellar medium and interstellar radiation field, and an isotropic presumably extragalactic diffuse emission, the extragalactic gamma-ray background (EGRB). The EGRB is a superposition both individual unresolved point sources and truly diffuse emission, encodes information about high energy processes in the universe and it is either non thermal or exotic. Thus, understanding the components of the EGRB is essential in order to constrain exotic high energy physics.

Gamma-rays have the smallest wavelengths and the most energy of any wave in the electromagnetic spectrum. High-energy particles can produce gamma-rays by the mechanisms of bremsstrahlung, inverse Compton scattering and synchrotron radiation. Such energetic particles are derived by jets of black holes, intense magnetic fields of neutron stars and pulsars, as well as supernovae explosions.

In Figure 1.1 we see the entire sky at energies between 100 MeV and 820 GeV based on seven years of data from the Large Area Telescope (LAT) instrument on NASA's Fermi Gamma-ray Space Telescope. Brighter colors indicate brighter gamma-ray sources. The image is in galactic coordinates so, in the center of the map is the center of the Milky Way and the plane of our galaxy is oriented horizontally across the middle (galactic plane). Above and below the bright band, much of the gamma-ray light comes from outside of our galaxy.

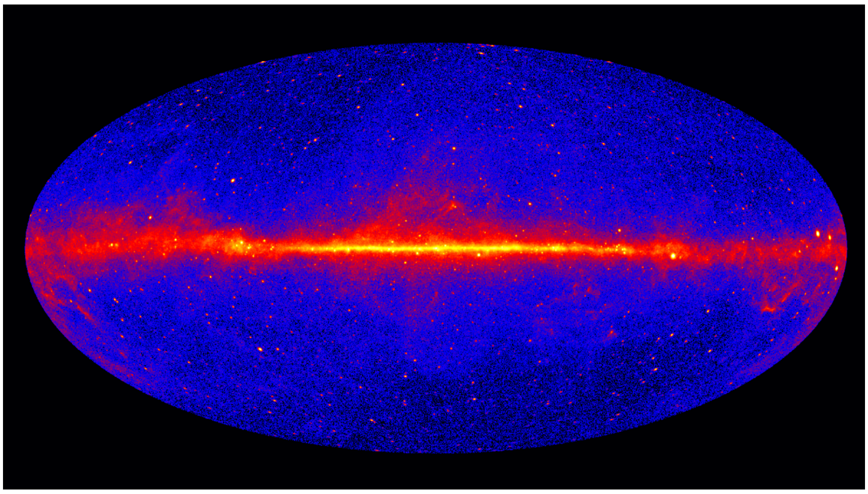

Figure 1.1: Gamma-Ray sky at energies above 1 GeV (Image Credit: NASA/DOE/Fermi LAT Collaboration).

After the analysis of the data taken by the Fermi LAT through the years, Fermi LAT collaboration creates source catalogues. The first Fermi LAT source catalogue is shown in Figure 1.2 and was obtained after one year of operation. The most recent one is the third source point catalogue after four years of operation.

The dominant components of the EGRB are likely active galaxies (blazars), which are the brightest extragalactic sources and the most numerous population of resolved gamma-ray sources,

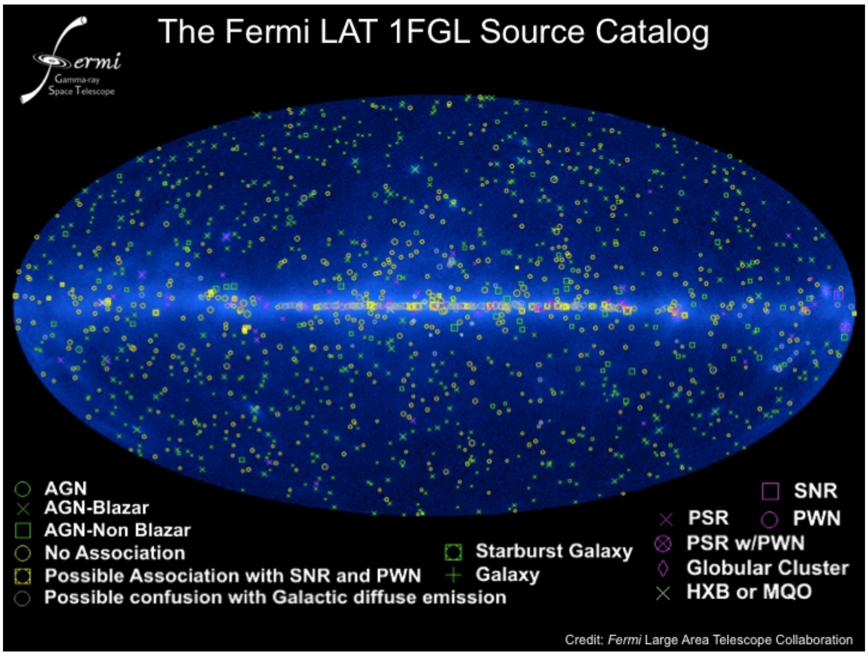

Figure 1.2: All point sources from the first Fermi LAT source catalogue (Image Credit: Fermi LAT collaboration).

and normal star-forming galaxies. These two classes of gamma-ray sources are guaranteed to contribute to the EGRB. It is believed that unresolved blazars are responsible for $\sim 20\%$ of the Fermi LAT measurement of the EGRB (Ackermann et al. (2015)). Blazars produce gamma-rays via the interactions of relativistic electrons with photons by the mechanism of inverse compton. These relativistic electrons acquire their energy via the process of Fermi acceleration: shocks within the jets move back and forth in the magnetic lines. The photons are emitted by electrons via synchrotron emission or from accretion disk emission. Another process with which blazars produce gamma-rays are from photopion production. Relativistic protons interact with photons and emit neutral pions, which then decay to gamma rays.

The normal star-forming galaxies contribution to the extragalactic gamma-ray background (EGRB) has been extensively studied and is one of the major objectives of the Fermi Gamma-Ray Space Telescope survey, as calculating and subtracting the most dominant sources of the EGRB will help us identify and study more exotic ones which might lead to the discovery of new physics. In normal star-forming galaxies the dominant emission mechanism of gamma-rays is through the interaction between cosmic-rays and interstellar gas, i.e.,

$$p_{\rm cr} + p_{\rm ism} \rightarrow pp\pi^0 \tag{1.1}$$

Then, gamma-rays are produced by the decay of the neutral pion (Stecker (1971)),

$$\pi^0 \rightarrow \gamma\gamma \tag{1.2}$$

Then the flux of gamma-rays will then depend on: a) the flux of projectiles (cosmic rays) and b) the number of targets. It is guaranteed that they contribute since there are numerous galaxies and if one galaxy is star-forming one this means that there is a lot of gas. Thus, there is a significant amount of targets for the cosmic rays to interact with (equation (1.1)). There are cosmic rays because there is star-formation. It is believed that supernovae remnants are the accelerators of cosmic rays in galaxies. Hence, star-forming galaxies have all the necessary ingredients to produce gamma-rays.

The contribution of misaligned active galactic nuclei (AGN) and millisecond pulsars was also calculated but it is significantly smaller than blazars and SFGs (see Fornasa & Sánchez-Conde (2015) and references therein). Misaligned AGNs produce gamma-rays with the same mechanisms as blazars but they are fainter since, they are not beamed towards us. Millisecond pulsars due to their huge magnetic field (up to 10^{12}G, can cause protons to emit synchrotron radiation. Several other candidates contributing to the EGRB have been proposed, with the most popular being clusters of galaxies, gamma-ray bursts and radio-quiet AGNs. The study of EGRB can also be essential to the comprehension of more exotic contributors, since, for example, it can broaden our understanding of the nature of dark matter: dark matter particles can emit gamma-rays through annihilation or decay and following various mechanisms depending on the dark matter candidate (Bertone et al. (2005)).

In this work, we solely focus on the contribution of normal star-forming galaxies to the EGRB. This contribution has been studied extensively by, e.g., Pavlidou & Fields (2002), Fields et al. (2010), Makiya et al. (2011), Stecker & Venters (2011) and Ackermann et al. (2012). Pavlidou & Fields (2002) and Ando & Pavlidou (2009) used the global star-formation-rate (SFR) density as a cosmic ray acceleration indicator (if galactic cosmic rays are accelerated in supernovae remnants) and assumed closed box galaxies to calculate the evolution of gas. Fields et al. (2010) starting from first principles, constructed a relation between star-formation rate, gamma-ray luminosity and gas content in a galaxy which allowed them to calculate the gamma-ray luminosity function of star-forming galaxies. Stecker & Venters (2011) calculated the contribution from unresolved star-forming galaxies considering three different models, each one with different assumptions. The first model considered a Schecter function and an evolving gas fraction. In the second model the contribution was determined from IR luminosity functions and in the third one from cosmic SFR and star-formation efficiency.

Ackermann et al. (2012) estimated the collective intensity of unresolved star-forming galaxies at redshifts $0 < z < 2.5$. They used empirical scaling relation between gamma-ray luminosity and total infrared (TIR), which they derived using two different regression methods to their sample (SMC, LMC, M31, Milky Way, NGC 253, NGC 4945, M82, and NGC 1068). Two galaxies of their sample are detected with AGN (NGC 4945 and NGC 1068) so, we have to exclude them. Their result for the contribution of normal star-forming galaxies to the EGRB is shown in Figure 1.3, where they have used a power-law spectral model of photon index 2.2 for energies above 0.3 GeV.

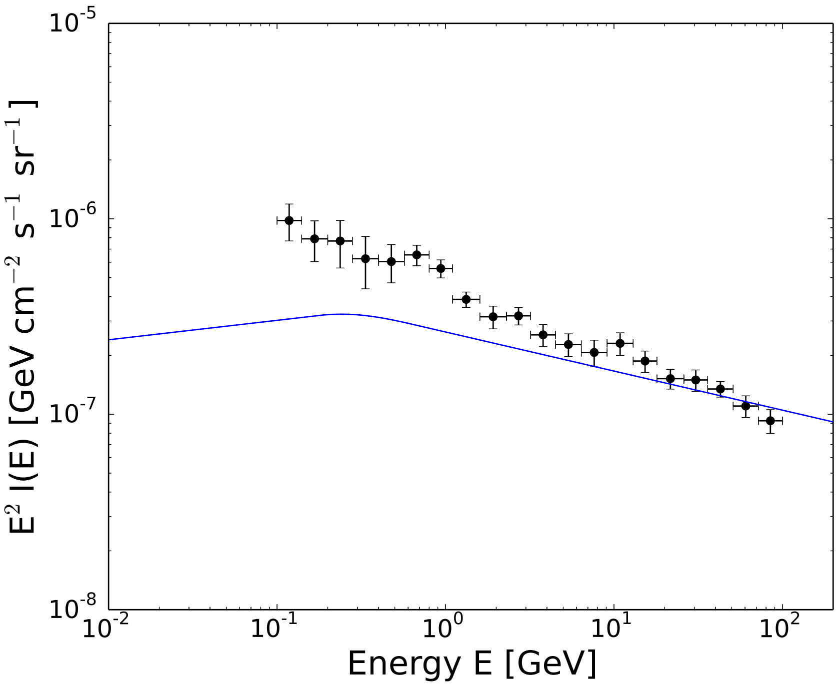

Figure 1.3: The result of Ackermann et al. (2012), who considered a scaling relation between L_γ and L_{TIR} with no other dependences. Fermi data are from (Ackermann et al. (2015)).

However, there is still no consensus in all the results of these different approaches. The difference is not just arithmetical, there is tension between theoretical expectation and empirical correlation between SFR and gamma-ray luminosity (L_γ). The slope of the relation between L_γ and total infrared luminosity ($L_{8-1000\mu m}$) is 1.714 according to the theoretical approach (Fields et al. (2010)) and 1.09 according to the empirical expression (Ackermann et al. (2012)).

In this work, our main goal is to understand the origin of this discrepancy on the slope and to set realistic bounds to the contribution of normal star-forming galaxies that are correctly allowed by observational input. We examine all possible sources of discrepancy, including redshift (z) dependence. Since, the amount of available gas in a galaxy will be a function of redshift, so will be the number of pions produced. Thus, the production of gamma-rays through the pion decay will vary with time. Hence, it is expected that the relation between L_γ and $L_{8-1000\mu m}$ will also be a function of redshift.

Moreover, we use SFR indicators to make our result more accurate by correcting it with the star-formation history $\dot{\rho}_*$ of Hopkins & Beacom (2006). We also take into consideration the effect of low number statistics on the empirical slope of L_γ and L_{SFR} indicator and finally, we take into account the dependence of the metallicity and we try to determine the possible effects it will have in our results.

The metallicity (Z) is the fraction of mass of a star that is not in hydrogen or helium. The word “metals” refers to all other elements except hydrogen and helium. Stars and nebulae with high abundances of carbon, nitrogen and oxygen for example, are called metal-rich. Metallicity is a good estimator of the chemical abundances of stars, which change over time by the mechanisms of stellar evolution. Thus, measuring the metallicity of a star can approximately indicate its age.

It is well known that the Universe is chemically evolving. The early Universe was metal-poor since, it was consisted of hydrogen and helium. The heavier elements were generated in the universe, by the stellar winds of stars or their explosions as supernovae. Through the process of star evolution stars synthesised metals from hydrogen and helium via the process of nucleosynthesis, which also constitute their energy supplier. Therefore, it is believed that older generations of stars generally have lower metallicities than those of younger generations.

However, we cannot measure the metallicity of stars but instead we measure the metallicity of the gas in galaxy, i.e., the metallicity of the interstellar medium. Thus, we measure the chemical composition of galaxies which, ultimately, will help us understand how galaxies are evolving. As galaxies evolve, star-formation converts gas into stars, which as we mentioned above, produce heavier elements via nuclear reactions and then expel them into the surrounding medium. Hence, the metallicity of a galaxy is an important indicator of the evolutionary history of a galaxy.

So, metallicity affects star-formation and vice versa. But, the gamma-ray luminosity of a galaxy depends on the star-formation rate of the galaxy. Thus, there must be a relation between gamma-ray luminosity and metallicity. The first who discovered a relationship between luminosity and metallicity was Lequeux et al. (1979). Then, various studies confirmed that such a relation or a relation between stellar mass and metallicity should exist (e.g. Rubin et al. (1984); Skillman et al. (1989)). We will also use a similar relation to derive the scaling relation between gamma-ray luminosity and TIR luminosity of a galaxy as a function of redshift and metallicity.

Chapter 2

Model

In order to compute the collective intensity of unresolved star-forming galaxies we use the line-of-sight integral (Ackermann et al. (2012)) over the gamma-ray luminosity function:

$$I(E_0) = \int_0^{z_{\max}} \int_{L_{\gamma,\min}}^{L_{\gamma,\max}} \Phi(L_\gamma, z) \frac{d^2V}{dz d\Omega} \frac{dN}{dE} \left(L_\gamma, E_0(1+z)\right) dL_\gamma dz \tag{2.1}$$

where E_0 is the observed photon energy. The function $\Phi(L_\gamma, z) = d^2N/dVdL_\gamma$ is the infrared luminosity function. $dN/dE(L_\gamma, E_0(1+z))$ is the differential photon flux of an individual galaxy with integrated gamma-ray luminosity L_γ at redshift z and $dV^2/dzd\Omega$ expresses the comoving volume element per unit redshift and unit solid angle.

The luminosity function that we must use is actually the gamma-ray luminosity function. However, we cannot determine it from Fermi data on resolved star-forming galaxies because these are too few. So, in order to estimate it we use an infrared luminosity function and then rescale it to gamma-ray luminosity L_γ. Hence, most of the uncertainty in the calculation of the contribution of normal star-forming galaxies to the EGRB enters through the luminosity function $\Phi(L_\gamma, z)$. There are various models about how to rescale the infrared luminosity function, which lead to different results.

Ackermann et al. (2012) obtained the different scaling relations between wavebands by fitting simple power law forms. They used the following relation between gamma-ray and TIR luminosity:

$$\log\left(\frac{L_{0.1-100\mathrm{GeV}}}{\mathrm{erg\ s^{-1}}}\right) = \alpha \log\left(\frac{L_{8-1000\mu\mathrm{m}}}{10^{10} L_\odot}\right) + \beta \tag{2.2}$$

They find α and β using two algorithms. The first one is the Expectation-Maximization (EM) algorithm (e.g., Dellaert (2002) and references therein), which is similar to the well known least-square fitting. For the full sample of galaxies, $\alpha = 1.17 \pm 0.07$ and $\beta = 39.28 \pm 0.08$, while excluding the ones with AGN (NGC 4945 and NGC 1068) $\alpha = 1.09 \pm 0.10$ and $\beta = 39.19 \pm 0.10$. The second one is the Buckley-James algorithm (Buckley and James, (1979)), where $\alpha = 1.18 \pm 0.10$ and $\beta = 39.31$ for the full sample. Excluding the galaxies with AGN, $\alpha = 1.10 \pm 0.14$ and $\beta = 39.22$.

We examine and quantify possible sources of uncertainty that can enter through this scaling. As a first step we include the dependence of the gamma-ray luminosity (L_γ) of a galaxy from redshift (z) and SFR (ψ), as we explained above, so,

$$L_\gamma = L_\gamma(z, \psi) \tag{2.3}$$

By adopting the scaling of gamma-ray luminosity with a galaxy's gas mass and SFR ψ (Pavlidou & Fields (2001)):

$$L_\gamma \propto M_{\mathrm{gas}} \Phi_{\mathrm{cr}} \tag{2.4}$$

we can determine the gamma-ray luminosity of any star-forming galaxy, assuming that the initial mass function (IMF) and the confinement are constant. The normalization constant can be derived by normalizing to the Milky Way, since, the local cosmic-ray flux and the global star-formation rate is well measured. Moreover, we take the gamma-ray production rate per interstellar H-atom, $\Gamma_{\pi^0 \to \gamma\gamma}$, to be proportional to the galaxy's volume averaged cosmic-ray proton flux, Φ_p (Pohl

(1994); Persic & Rephaeli (2010)) and by assuming that the ratio of cosmic-ray flux to SFR will be constant for all normal star-forming galaxies, we have that:

$$\frac{\Gamma_{\pi^0\to\gamma\gamma}}{\Gamma^{\mathrm{MW}}_{\pi^0\to\gamma\gamma}} = \frac{\Phi_{\mathrm{cr}}}{\Phi^{\mathrm{MW}}_{\mathrm{cr}}} = \frac{R_{\mathrm{SN}}}{R^{\mathrm{MW}}_{\mathrm{SN}}} = \frac{\psi}{\psi_{\mathrm{MW}}} \tag{2.5}$$

Thus,

$$L_\gamma \propto M_{\mathrm{gas}}\psi \tag{2.6}$$

We should now specify the gas mass of a galaxy. From the Kennicutt-Schmidt law (Schmidt (1959); Kennicutt (1998)),

$$\sum\nolimits_{\mathrm{SFR}} = A \sum\nolimits^{x}_{\mathrm{gas}} \tag{2.7}$$

we can deduce the interstellar gas mass of a galaxy at a given star-formation rate:

$$M_{\mathrm{gas}}(\psi, z) = 2.8 \times 10^9 M_\odot (1+z)^{-\beta} \left(\frac{\psi}{1 M_\odot \mathrm{yr}^{-1}}\right)^{\omega} \tag{2.8}$$

where, $\beta = 2(1 - 1/x)$ and $\omega = 1/x$ and x is the slope of the Kennicutt-Schmidt law (Fields et al. (2010)). The term $(1+z)^{-\beta}$ enters through the conversion of surface densities of gas and SFR in the KS law to volume densities.

Hence, following the formalism of Fields et al. (2010), it is easy to show that the gamma-ray luminosity of a galaxy will be,

$$L_\gamma\,(\psi, z) \propto (1+z)^{-\beta} \left(\frac{\psi}{M_\odot \mathrm{yr}^{-1}}\right)^{\omega+1} \tag{2.9}$$

However, this equation is valid only for normal escape-dominated galaxies. Starburst galaxies have very high cosmic-ray intensities within small volumes where inelastic collisions compete with and sometimes even dominate, outflows to regulate cosmic-rays losses (Paglione et al. (1996); Lacki et al. (2010); Torres et al. (2004); Thompson et al. (2007); Persic & Rephaeli (2010); Stecker (2007)), thus we have to exclude them.

The total infrared luminosity is a well-established tracer of the SFR (ψ) for late type galaxies (Kennicutt (1998a)). The conversion proposed by Kennicutt (1998b) is the following one:

$$\frac{\psi}{1 M_\odot \mathrm{yr}^{-1}} = \epsilon 1.7 \times 10^{-10} \frac{L_{8-1000\mu m}}{L_\odot} \tag{2.10}$$

This conversion assumes that thermal emission of interstellar dust approximates a calorimetric measure of radiation produced by young, i.e. $10 - 100$ Myr, stellar populations. The factor ϵ depends on the assumed initial mass function (IMF). Throughout this work we use Salpeter IMF (Salpeter (1955)) and we consider it unchanging through space and time ($\epsilon = 1$).

Hence, the scaling relation between gamma-ray luminosity and TIR luminosity is obtained by substituting equation (2.10) into equation (2.9),

$$L_\gamma(L_{8-1000\mu m}, z) \propto (1+z)^{-\beta} \left(\frac{L_{8-1000\mu m}}{L_\odot}\right)^{\omega+1} \tag{2.11}$$

Equation (2.11) serves as the basis of our model. In order then to calculate $\Phi(L_\gamma, z)$, which enters equation (2.1), all that is needed is to a) adopt a luminosity function, b) determine the slopes β and ω (either from KS law or empirically) and c) determine the normalization of the scaling in equation (2.11).

In the model of Ackermann et al. (2012) eight galaxies are used in order to derive the scaling relation between the gamma-ray luminosity and TIR luminosity of a galaxy. However, two of them (NGC 4945 and NGC 1068) are galaxies with active galactic nuclei (AGN) so, we are not going to consider them in this work. Our sample of galaxies consists of four normal star-forming galaxies (SMC, LMC, MW, M31) and four starburst (NGC 253, M82, NGC 2146, and Arp 220) whose effects to our results will be examined later. For our calculation, we adopt a power-law spectral model with photon index 2.33, which is the average of all photon indices of the normal star-forming galaxies in our sample. For normal and starburst galaxies we use photon index 2.27.

2.1 Infrared Luminosity Function

We begin by considering the adopted luminosity function. Fields et al. (2010) use an Hα luminosity function while Ackermann et al. (2012) use the luminosity function of Rodighiero et al. (2010):

$$\Phi(L)\mathrm{dlog}_{10}(L) = \Phi^* \left(\frac{L}{L^*}\right)^{1-\alpha} \exp\left[-\frac{1}{2\sigma^2}\log_{10}^2\left(1+\frac{L}{L^*}\right)\right] \mathrm{dlog}_{10}(L) \tag{2.12}$$

where, the parameter α correspond to the slope at the faint end, L^* is the characteristic $L_{\mathrm{bol}}^{\mathrm{IR}}$ luminosity and finally, Φ^* is the normalization factor.

However, the cosmic SFR that arises by adopting these luminosity functions are in poor agreement with the star-formation history $\dot{\rho}_*$ reported by Hopkins & Beacom (2006), which is currently the best available determination of the cosmic SFR history, taking into account information from all available SFR tracers.

In order to bring the IR luminosity function used in agreement with the CSFR history of Hopkins & Beacom (2006) we adopt the following procedure: We adopt the luminosity function of Rodighiero et al. (2010) but we introduce a redshift-dependent dimensionless normalization correction factor in the scaling of equation (2.10):

$$\frac{\psi}{1M_\odot\mathrm{yr}^{-1}} = \epsilon 1.7\times10^{-10}h(z)\frac{L_{8-1000\mu m}}{L_\odot} \tag{2.13}$$

such that, $\int \psi\Phi(\psi,z)\mathrm{dlog}_{10}\psi = \dot{\rho}_*$, where $\dot{\rho}_*$ is the Hopkins & Beacom (2006) cosmic star-formation history, and $\Phi(\psi,z)$ is the star-formation rate distribution function obtained by the luminosity function of equation (2.12) and the scaling of equation (2.13). In this way we obtain:

$$h(z) = \begin{cases} 0.7\frac{0.017+0.13z}{\left[1+\left(\frac{z}{3.3}\right)^{5.3}\right](0.022\exp(1.77z)-0.015)} & 0<z<1 \\ 6.36\frac{0.017+0.13z}{1+\left(\frac{z}{3.3}\right)^{5.3}} & z>1 \end{cases} \tag{2.14}$$

The cosmic star-formation history as a function of redshift is shown in Figure 2.1. The function $h(z)$ is the appropriate function so that the red line and the black dots are in agreement with the blue line.

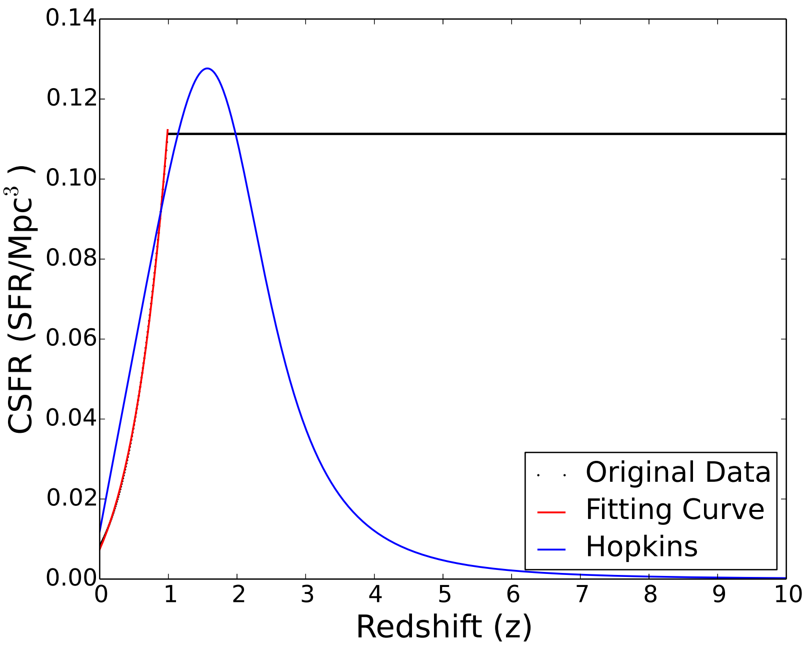

Figure 2.1: The difference between the cosmic star-formation history of Hopkins & Beacom (2006) and the one that arises from integrating the luminosity function of Rodighiero et al. (2010). The black dots (original data) represent the result of the integration. The blue line is the cosmic star-formation history of Hopkins & Beacom (2006) and the red line is the best-fit I performed in the result of the integration for $z<1$.

2.2 Comoving Volume Element

In order to define the comoving volume element we must first define some other parameters. We will begin from the basics and then, we will see the different ways we can use to specify a distance between two points, in cosmology.

First of all, the Hubble constant H_0 is the constant of proportionality between recession speed v and distance d in the expanding Universe, i.e:

$$v = H_0 d \tag{2.15}$$

In general, however, H is a function of time, so H_0 is actually the Hubble constant in the present epoch and we take H_0 to be equal to $H_0 = 73$ km Mpc^{-1} sec^{-1}. The inverse of the Hubble constant is the Hubble time t_H:

$$t_H \equiv \frac{1}{H_0} \tag{2.16}$$

and the speed of light c times the Hubble time is the Hubble distance D_H:

$$D_H \equiv c\, t_H = \frac{c}{H_0} \tag{2.17}$$

Another important parameter in cosmology is the critical density, $\rho_c(t)$, which is the value of the density that will result in a flat Universe ($k = 0$ in Friedman-Robertson-Walker (FRW) equations):

$$\rho_c(t) = \frac{3H^2(t)}{8\pi G} \tag{2.18}$$

hence, its present value, $\rho_{c,0}(t)$, is equal to:

$$\rho_{c,0} = \frac{3H_0^2}{8\pi G} \tag{2.19}$$

The ratio of a measured density to the critical density is called the density parameter and is defined as follows:

$$\Omega(t) = \frac{\rho(t)}{\rho_c(t)} \tag{2.20}$$

which is of course dimensionless.

We can now define three such density parameters. The first one is the mass density parameter, which is the mass density (of all types of matter) ρ of the Universe and equal to:

$$\Omega_M = \frac{8\pi G}{3H_0^2}\rho_0 \tag{2.21}$$

The second one is the density parameter of the cosmological constant Λ, which is equal to:

$$\Omega_\Lambda = \frac{\Lambda c^2}{3H_0^2} \tag{2.22}$$

Finally, the last one is the curvature density parameter Ω_k, which measures the curvature of space and can be defined by the following relation:

$$\Omega_M + \Omega_\Lambda + \Omega_k = 1 \tag{2.23}$$

or from FRW equations it can be found that it is equal to:

$$\Omega_k = -\frac{kc^2}{a_0^2 H_0^2} \tag{2.24}$$

and the possible values of k are: $k = 0, \pm 1$.

Due to the expansion of the Universe the distances between comoving objects are constantly changing and Earth bound observers look back in time as they look back in distance. As a result there are many ways to specify the distance between two points as we have already mentioned. Here we will examine each one of these ways separately since we will need almost all of them.

- **Comoving Distance (line-of-sight)**

  Suppose two nearby objects in the Universe that are moving with the Hubble flow. A small comoving distance δD_C is the distance between them which remains constant with epoch. Thus, it is the proper distance divided by the ratio of the scale factor of the Universe then to now, or equivalently it is the proper distance multiplied by $(1+z)$. In order to compute the total line-of-sight comoving distance D_C we have to integrate all the infinitesimal δD_C contributions between these events along the radial ray from $z=0$ to the object.

  Now, we define the following function

$$E(z) \equiv \sqrt{\Omega_M(1+z)^3 + \Omega_k(1+z)^2 + \Omega_\Lambda} \tag{2.25}$$

  which is proportional to the time derivative of the logarithm of the scale factor with redshift z and density parameters as defined above (Peebles, (1993)). In this way, the Hubble constant for an astronomer at redshift z is measured to be $H(z) = H_0\ E(z)$ and the Hubble distance is then:

$$D_H(z) = \frac{c}{H(z)} \Rightarrow D_H(z) = \frac{D_H}{E(z)} \tag{2.26}$$

  The total line-of-sight comoving distance is given by the following equation:

$$D_C = D_H \int_0^z \frac{dz'}{E(z')} \tag{2.27}$$

- **Comoving Distance (transverse) or Coordinate Distance**

  The transverse comoving distance or, as we will prefer to call it, coordinate distance D_M is the distance between two objects at the same redshift or distance but separated on the sky by some angle $\delta\theta$. It is related to the line-of-sight comoving distance D_C as follows (Weinberg, (1972); Peebles, (1993)):

$$D_M = \begin{cases} D_H \dfrac{1}{\sqrt{\Omega_k}} \sinh\left[\sqrt{\Omega_k}\dfrac{D_C}{D_H}\right] & \text{for } \Omega_k > 0 \\ D_C & \text{for } \Omega_k = 0 \\ D_H \dfrac{1}{\sqrt{|\Omega_k|}} \sin\left[\sqrt{|\Omega_k|}\dfrac{D_C}{D_H}\right] & \text{for } \Omega_k < 0 \end{cases} \tag{2.28}$$

- **Angular Diameter Distance**

  The angular diameter distance D_A is defined as the ratio of an object's physical transverse size to its angular size as viewed from Earth (in radians) and it is related to the coordinate distance as (Weinberg, (1972); Peebles, (1993))

$$D_A = \frac{D_M}{1+z} \tag{2.29}$$

- **Luminosity Distance**

  The luminosity distance D_L is defined by the relationship between bolometric flux S and bolometric luminosity L:

$$D_L \equiv \sqrt{\frac{L}{4\pi S}} \tag{2.30}$$

  and in terms of the coordinate distance and angular diameter distance it is (Weinberg, (1972))

$$D_L = (1+z)D_M = (1+z)^2 D_A \tag{2.31}$$

Finally, we are ready to define the comoving volume element. The comoving volume V_C is the volume measure in which number densities of non-evolving objects locked into Hubble flow are constant with redshift. We have seen that the derivative of comoving distance with redshift is $1/E(z)$ and that the angular diameter distance converts a solid angle $d\Omega$ into a proper area. We also now that two factors of $(1+z)$ convert a proper area into a comoving area so, the comoving volume element in solid angle $d\Omega$ and redshift interval dz is (Weinberg, (1972))

$$dV = D_H \frac{(1+z)^2 D_A^2}{E(z)} dz d\Omega \tag{2.32}$$

Until now, we have seen all the parameters we need but in the most general case. We use a standard ΛCDM cosmology with $\Omega_M = 0.3,\ \ \Omega_\Lambda = 0.7,\ \ H_0 = 73$ km Mpc^{-1} sec^{-1}.

So, for our case, Ω_k should be equal to zero, since $\Omega_M + \Omega_\Lambda = 1$. This will simplify our equations and all the different distances we have seen above. Thus, the comoving volume element is equal to

$$dV = D_H \frac{(1+z)^2 D_A^2}{\sqrt{0.3(1+z)^3 + 0.7}} dz d\Omega \tag{2.33}$$

2.3 Differential Photon Flux

We have seen the luminosity function they have used to obtain the collective intensity of the unresolved star-forming galaxies and how to calculate the comoving volume element, so the last unknown we need to specify is the differential photon flux.

We will follow Peacock ("Cosmological Physics", (2010)) as well as his notation. As he says, the most important relation in for observational cosmology is probably the relation between monochromatic flux density and luminosity:

$$S_\nu(\nu_{\rm obs}) = \frac{L_\nu\left([1+z]\nu_{\rm obs}\right)}{4\pi R_0^2 S_k^2(r)(1+z)} \tag{2.34}$$

but, luminosity distance is defined as

$$D_L = (1+z) R_0 S_k(r) \tag{2.35}$$

hence, monochromatic flux density can be written in the following form:

$$S_\nu(\nu_{\rm obs}) = \frac{L_\nu\left([1+z]\nu_{\rm obs}\right)}{4\pi D_L^2}(1+z) \tag{2.36}$$

or equivalently:

$$S_\nu(\nu_{\rm obs}) = L_{\nu_0}\left(\frac{(1+z)E_{\rm obs}}{E_0}\right)^{-\gamma} \frac{(1+z)}{4\pi D_A^2 (1+z)^2}$$

$$\Leftrightarrow S_\nu(\nu_{\rm obs}) = L_{\nu_0}\left(\frac{(1+z)E_{\rm obs}}{E_0}\right)^{-\gamma} \frac{1}{4\pi D_A^2 (1+z)} \tag{2.37}$$

where, we have also used equation (2.31). Now we will change the frequency interval into energy interval, in order to be able to replace L_{ν_0} with the gamma-ray luminosity L_γ, which is known. Thus,

$$S_E(E_{\rm obs}) = L_{E_0}\left(\frac{(1+z)E_{\rm obs}}{E_0}\right)^{-\gamma} \frac{1}{4\pi D_A^2 (1+z)} \tag{2.38}$$

All that is left, is to express L_{E_0} in terms of gamma-ray luminosity L_γ and we can do that as follows:

$$L_\gamma = L_{E_0} \int_{E_0 = 0.1\rm GeV}^{\infty} \left(\frac{E}{E_0}\right)^{-\gamma} dE \tag{2.39}$$

since, we are interested for photons with energy above $E_0 = 0.1$ GeV. Thus, we have the following relation between the luminosities:

$$L_{E_0} = \frac{(\gamma - 1)}{E_0} L_\gamma \tag{2.40}$$

Finally, we have that the flux density, assuming a power law spectral model with any photon index γ, is equal to:

$$S_E(E_{\rm obs}) = \frac{(\gamma-1)L_\gamma}{4\pi D_A^2(1+z)}\left(\frac{(1+z)E_{\rm obs}}{E_0}\right)^{-\gamma} \tag{2.41}$$

hence,

$$I(E_{\rm obs}) = \frac{E_{\rm obs}(\gamma-1)L_\gamma}{4\pi D_A^2(1+z)}\left(\frac{(1+z)E_{\rm obs}}{E_0}\right)^{-\gamma} \tag{2.42}$$

since by definition it is:

$$S_E(E_{\rm obs}) \equiv I(E_{\rm obs})E_{\rm obs} \tag{2.43}$$

2.4 Scaling slopes ω & β

Perhaps the most puzzling discrepancy between the theoretical approach of Fields et al. (2010) and the empirical scaling of Ackermann et al. (2012) is the discrepancy in the scaling slope $\omega + 1$ between L_γ and ψ.

From a physics perspective, if $L_{8-1000\mu m}$ is indeed proportional to ψ (and is not also modulated by the gas content of a galaxy), the $L_\gamma - L_{8-1000\mu m}$ *should* deviate significantly from unity to reflect the compounded effect of both star-formation ($\rightarrow$ cosmic ray accelerators $\rightarrow$ flux of projectiles) and gas ($\rightarrow$ availability of targets).

If the empirical scaling (even in the local universe) does indeed exclude a steeper slope, then this would have important implications: it could imply, for example, that confinement of cosmic rays in galaxies is not only variable, but star-formation dependent (with higher star-forming galaxies exhibiting poorer confinement properties); or that the IMF is star-formation dependent; or that any scatter in the $L_{8-1000\mu m}$ − SFR scaling is dependent on gas content, which could also explain why the additional effect of gas mass is "hidden" from the L_γ − SFR scaling if $L_{8-1000\mu m}$ is used as an SFR tracer; or finally, that the primary contribution in the γ − ray flux from star-forming galaxies is leptonic rather than hadronic and thus dependent on cosmic-ray flux but not on gas.

Before that scenarios are entertained, however, we need to test to what extend the extremely limited number of star-forming galaxies detected can indeed constrain the scaling slope. The effect of small-number statistics would enter not through the uncertainty of the fit to a power-law scaling, but through the incomplete sampling of scaling that is bound to have finite scatter.

To test this effect, we performed Monte carlo calculations to examine how the slope derived from a power-law fit is affected. We picked a random number, c, from normal distributions with different standard deviation (STD), meant to represent the scatter in the $L_\gamma - L_{8-1000\mu m}$ scaling. Then, for each L_γ and $L_{\rm TIR}$ we added that random number to a number of simulated data points equal to the real resolved star-forming galaxy sample drawn from scaling relations of the form (2.2), i.e.,

$$\log\left(\frac{L_{0.1-100\rm GeV}}{\rm erg\ s^{-1}}\right) = (\omega+1)\log\left(\frac{L_{8-1000\mu\rm m}}{10^{10}L_\odot}\right) + \alpha + c \tag{2.44}$$

where α is the normalization constant which results considering normal and starburst galaxies. We then fit the simulated data with a power-law and we examined how the STD of the slopes $(\omega + 1)$ depends on the STD of the normal distributions. The results are shown in Figure 2.2. If the $L_\gamma - L_{\rm TIR}$ scaling has a 1dec scatter, the 1σ spread of slopes would be ≈ 0.5.

Even when considering the starburst galaxies in our sample, our results are sensitive to the fact that we have low number statistics. The slope of the scaling relation between gamma-ray luminosity and TIR luminosity, that we use, has large uncertainties and depends on sample used. For this reason, at this stage a difference between $\omega + 1 = 1.7$ (L_γ dependent on $\psi M_{\rm gas}$) and $\omega + 1 = 1.1$ (L_γ dependent on ψ alone) cannot be confidently claimed due to the limited number of resolved star-forming galaxies in gamma-rays.

In this work, we will examine both best-fit values of $\omega+1$ using the latest data on Fermi-resolved star-forming galaxies, as well as other possible values of $\omega + 1$ between 1 (i.e., no effect of gas) and 2 (i.e., $\omega = 1/x = 1$, SFR$\propto$gas, maximum possible effect of gas).

The value of β is taken always to be consistent with that of ω, i.e., $\beta = 2(1 - \omega)$. However, the factor $(1 + z)^{-\beta}$ may not capture all relevant redshift dependent (in addition to those of Φ, $h(z)$). Another redshift-dependent effect may enter through the metallicity evolution of the average galaxy with redshift.

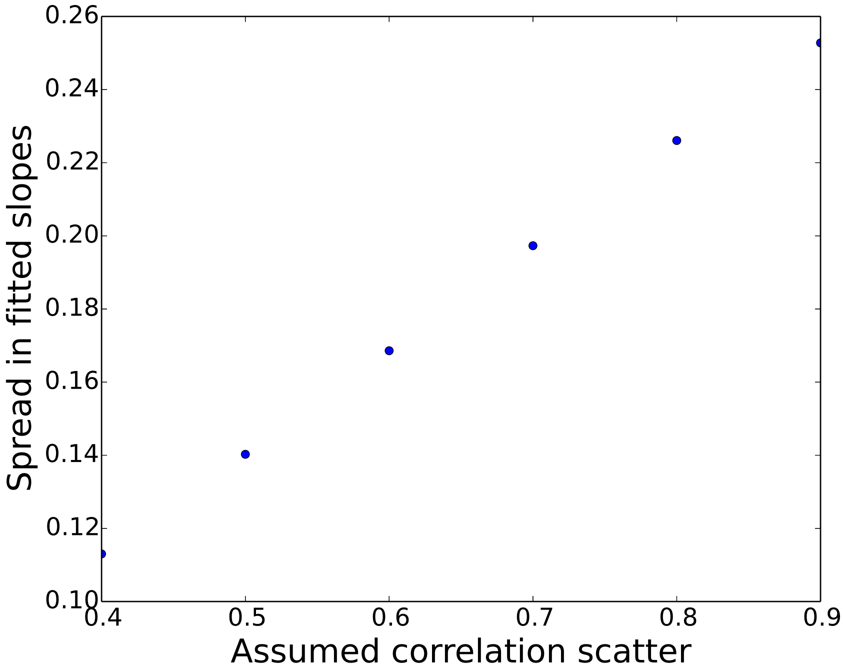

Figure 2.2: Dependence of the spread of possible slopes on the assumed scatter in the correlation.

One of the assumptions in Fields et al. (2010) is that the ratio of cosmic-ray flux to star-formation rate is constant for all normal star-forming galaxies. In general this is not true since, it can be a function of the metallicity (Z) and the IMF. In this work we considere a Salpeter IMF and we will explore the effects of metallicity. The metallicity can affect the minimum mass of a star that undergoes a supernovae explosion quantitatively. Thus, equation (2.5) becomes:

$$\frac{\Gamma_{\pi^0\to\gamma\gamma}}{\Gamma^{\mathrm{MW}}_{\pi^0\to\gamma\gamma}} = \frac{\Phi_{\mathrm{cr}}}{\Phi^{\mathrm{MW}}_{\mathrm{cr}}} = \frac{R_{\mathrm{SN}}}{R^{\mathrm{MW}}_{\mathrm{SN}}} = f(Z)\frac{\psi}{\psi_{\mathrm{MW}}} \tag{2.45}$$

where, $f(Z)$ is a general function that encodes the effects of metallicity.

In order to specify this general function $f(Z)$ we follow Ibeling & Heger (2013). They calculated the dependence of the low mass limit for making core-collapse supernovae (SNe) as a function of the initial stellar metallicity. Their main conclusion was that for a fixed IMF the SN rate may be $20\% - 25\%$ higher at $[Z] = -2$ than at $[Z] = 0$, where $[Z] = \log(Z/Z_\odot)$. We are interested in the minimum mass required for a star to undergo a classical core-collapse event not triggered by electron capture with the formation of an ONe degenerate core. Following the notation of Ibeling & Heger (2013), this mass is denoted by $M^{\mathrm{up}'}(Z)$. The relation they suggest for the metallicity dependent transition mass is:

$$\frac{M^{\mathrm{up}'}(Z)}{M_\odot} = \begin{Bmatrix} \sum_{i=0}^{6} \alpha_i [Z]^i & : [Z] \geq -8.3 \\ 9.19 & : [Z] < -8.3 \end{Bmatrix} \pm 0.15 \tag{2.46}$$

where the coefficients α_i are the best fit parameters after they parametrize it as sixth order polynomial. Salpeter IMF (Salpeter (1955)) is valid for a stellar mass range $0.1 - 120 M_\odot$. In order to correct for metallicity, we must divide the total number of stars that will undergo a supernovae explosion with the total number of stars. The total number of stars that will undergo supernovae can be computed by integrating the Salpeter IMF from $M^{\mathrm{up}'}(Z)/M_\odot$, to $M_{\max} = 120$. Hence, the general function $f(Z)$ mentioned above is proportional to:

$$f(Z) \propto \left(\frac{M^{\mathrm{up}'}(Z)}{M_\odot}\right)^{-1.35} \tag{2.47}$$

The next step into incorporating this z-dependence in equation (2.45) is to transform metallicity (Z) into redshift (z) in order to simplify our calculations and to derive the final scaling relation between the gamma-ray luminosity and the total infrared luminosity of a galaxy. According to the model of Kistler et al. (2013), the mettalicity evolves with redshift as follows:

$$Z(z) = 0.03 \times 10^{-0.15z} \tag{2.48}$$

Hence, using equations (2.48) and (2.46), we have $M^{\mathrm{up}'}(z)/M_{\odot}$.

2.5 Normalization of $L_{\gamma} - L_{\mathrm{TIR}}$ scaling

For each slope $\omega + 1$ that we will examine, we have to determine the normalization of the scaling of equation (2.11). We do so by performing least-squares fitting on the sample of resolved star-forming galaxies that are relevant in each case (normal or normal + starburst), while assuming that the scaling slope is fixed at the desired value. We call the normalization resulting in this way $L_{\gamma,0}(\omega)$.

Combining all the above effects we finally obtain the following expression of scaling relation between the gamma-ray luminosity and the total infrared luminosity of a galaxy:

$$L_{\gamma} = L_{\gamma,0}(\omega)(1+z)^{-\beta}\,(h(z))^{\omega+1}\left(\frac{M^{\mathrm{up}'}(z)}{M_{\odot}}\right)^{-1.35}\left(\frac{L_{8-1000\mu m}}{L_{\odot}}\right)^{\omega+1} \tag{2.49}$$

For example, in Figure 2.3 the result of the least-square fitting for the slope $\omega + 1 = 1$ is shown. The sample of galaxies are the four available normal star-forming galaxies.

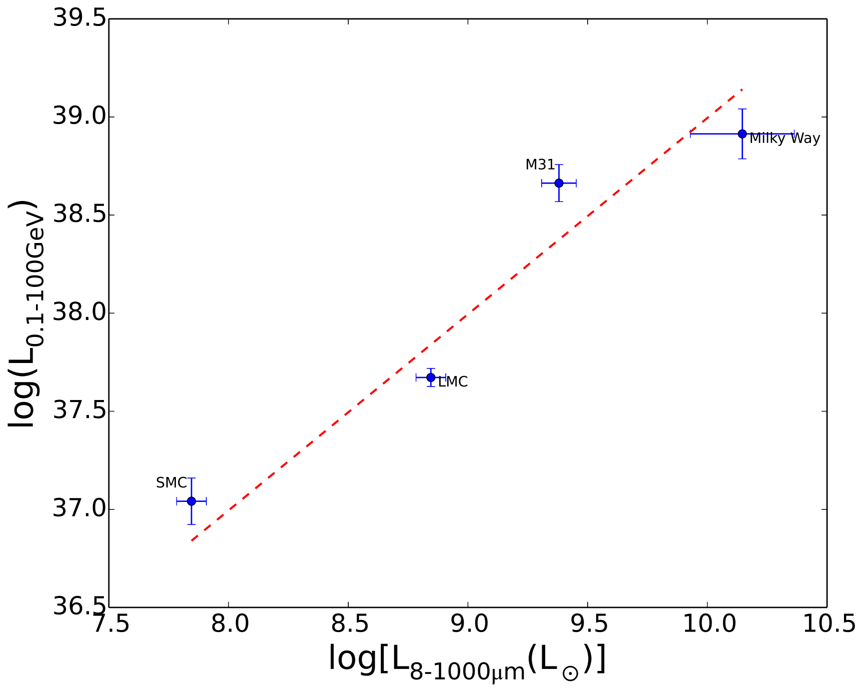

Figure 2.3: The result of the least-square fitting to the normal star-forming galaxies, for the desirable slope $\omega + 1 = 1$.

In Figure 2.4 it is again the result of the least-square fitting for the same slope but, considering the full sample of available galaxies.

In order to better clarify the calculation of the normalization constant, in Figure 2.5 it is shown the least-square fitting for the slope 1.714, i.e., $\omega + 1 = 1.714$ in the full sample of galaxies.

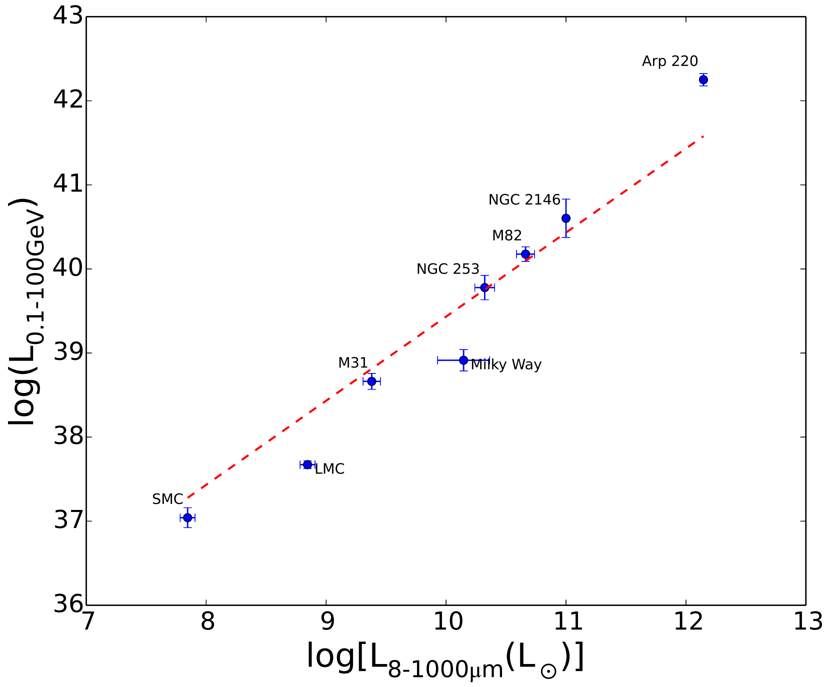

Figure 2.4: The result of the least-square fitting to the full sample of galaxies (normal and starburst ones), for the desirable slope $\omega + 1 = 1$.

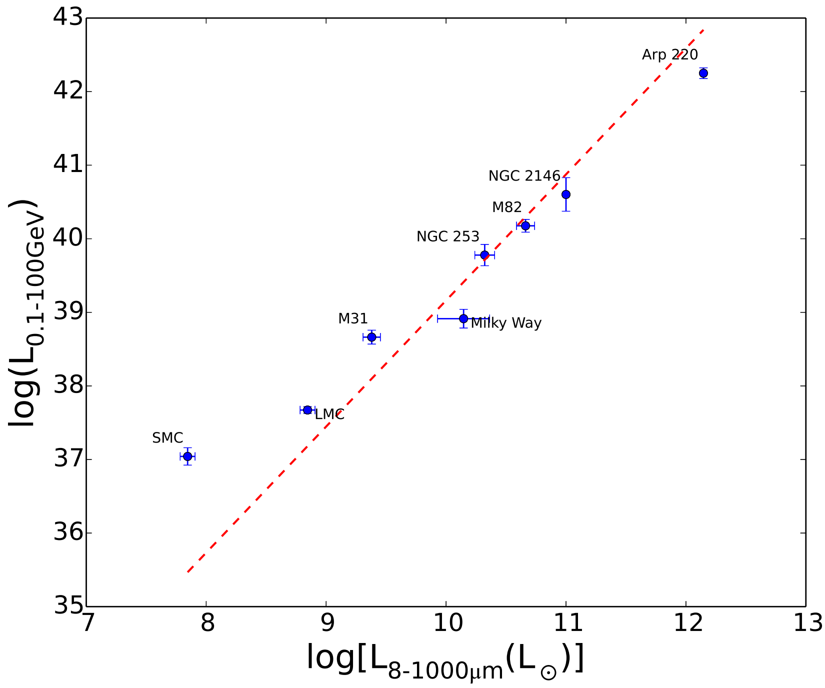

Figure 2.5: The result of the least-square fitting to the full sample of galaxies (normal and starburst ones), for the desirable slope $\omega + 1 = 1.714$. We can see the difference with the above Figure 2.4

Chapter 3

Results

In this section, we present the results we obtained for the contribution of normal star-forming galaxies to the EGRB using equation (2.49).

3.1 Effect of Metallicity

The effect of metallicity to the collective intensity of unresolved star-forming galaxies is shown in Figure 3.1. As we can see the metallicity does not affect our result appreciably, thus the ratio of cosmic-ray flux to SFR can be indeed assumed to be constant for all normal star-forming galaxies, if the IMF is constant. However, we note that our correction is made on an average sense and does not reflect the distribution of galaxy metallicities at a given z, nor the distribution of metallicities within a single galaxy.

Moreover, it is probable that, the dependence of IMF will contribute more significantly. Nonetheless, we do not consider this case here, since this would require altering different luminosity functions and to assume a non constant IMF. Further analysis of metallicity and IMF in general is required to conclude to a more solid result and to exclude some other possibilities.

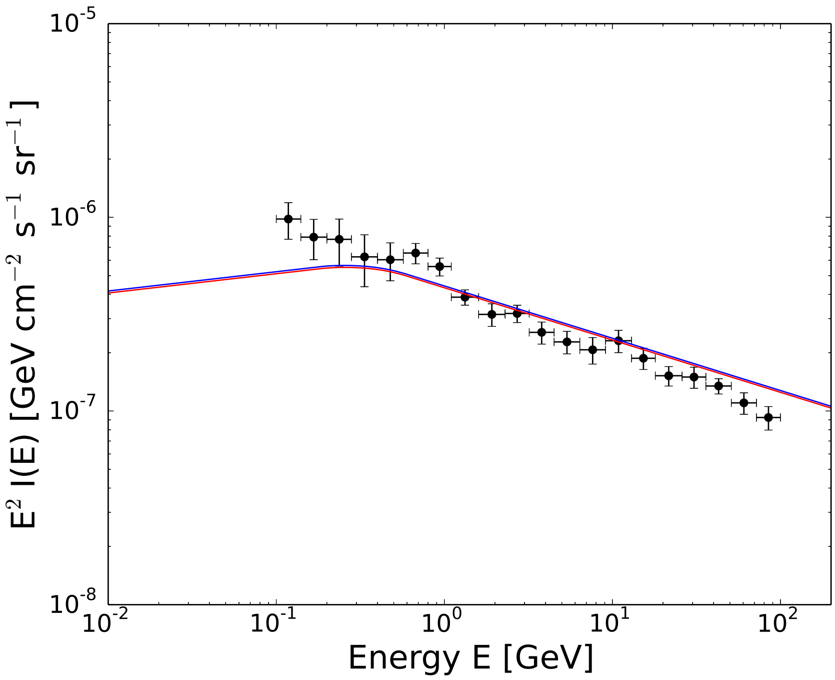

Figure 3.1: Metallicity effects to the contribution of unresolved star-forming galaxies to the isotropic diffuse gamma-ray emission measured by the Fermi LAT(black points, Ackermann et al.(2015)). The blue line represents our results with the metallicity considered in equation (2.49), while the red line without.

3.2 Normal Galaxies

In Figure 3.2 we estimate the normal star-forming galaxies contribution to the EGRB without considering the starburst galaxies. Hence, the normalization constants for each desirable slope, i.e., $\omega + 1$, are obtained using only the four normal star-forming galaxies. The different curves come from different values of ω and β in the equation (2.49).

The orange and the solid cyan lines represent the bounds of the possible contribution of normal star-forming galaxies to the EGRB. Their slopes are obtained for two extreme cases of the slope ω. The orange one is obtained for $\omega = 2$ ($x = 1$, i.e., one-to-one relation between the surface density of SFR and the surface density of gas). When the gas is increasing the amount of targets for proton-proton collisions is increasing. In contrast, the solid cyan line is obtained for $\omega = 1$ ($x = \infty$, i.e., the surface density of SFR and the surface density of gas are completely uncorrelated or equivalently the gas mass does not enhance the gamma-ray emission of a galaxy). These two extreme scenarios set the bounds to the possible contribution of normal star-forming galaxies to the EGRB.

Moreover, the green line in Figure 3.2 is obtained using a different star-formation tracer to determine empirically the slope $\omega+1$ from L_γ data: near-ultraviolet (NUV) plus $25\mu m$ luminosity of each galaxy, i.e., $\nu L_{\rm NUV} + 2.26 L_{25\mu m}$. From least-square fitting we got $\omega + 1 = 1.268$, i.e., $L_\gamma \propto (\nu L_{\rm NUV} + 2.26 L_{25\mu m})^{1.268}$. We examine this case because the NUV + MIR (Mid-Infrared) luminosity is better estimator of recent SFR than TIR luminosity, as the $25\mu m$ luminosity term corrects for possible existence of dust (Kennicutt & Evans(2012)). In this case, however, we do not consider the Milky Way in our sample, since we cannot measure its NUV luminosity. Hence, we perform least-square fitting using the three other normal star-forming galaxies (SMC, LMC, M31).

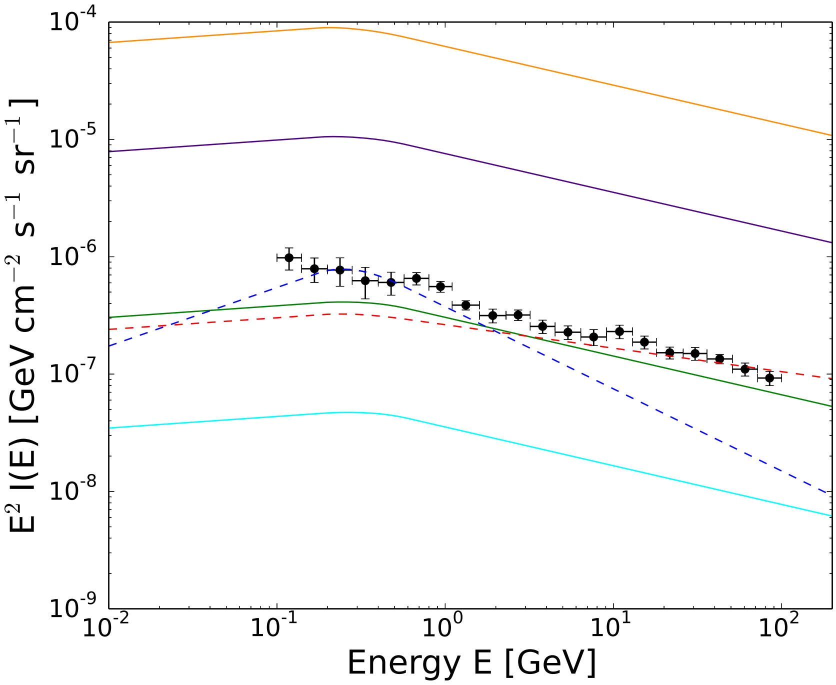

Figure 3.2: The contribution of normal star-forming galaxies to the extragalactic gamma-ray background and its possible bounds. *Orange* line represents the upper bound of the contribution while the *solid cyan* line the lower one. *Indigo* line is based on the analysis of Fields et al. (2010) but adding also the function $h(z)$. *Green* line is obtained using a scaling relation between L_γ and $\nu L_{\rm NUV} + 2.26 L_{25\mu m}$. The *red dashed* line is the result of Ackermann et al. (2012) and the *blue dashed* line is from Ando & Pavlidou (2009) (see text for details). Fermi data are from (Ackermann et al. (2015)).

The indigo line is based on formalism of Fields et al. (2010), where it is assumed that $x = 1.4$ and $\omega + 1 = 1.714$. This result is different from the result of Fields et al. (2010) since we have consider the additional redshift dependence $h(z)$ of the empirical SFR$-L_{8-1000\mu m}$ relation to ensure that the IR luminosity function yields a cosmic SFR history consistent with Hopkins & Beacom (2006). The red dashed line represents the result of Ackermann et al. (2012) and finally the blue dashed line the result of Ando & Pavlidou (2009), where they used the SFR density as a function of redshift instead of a luminosity function.

The indigo and orange lines are inconsistent with the EGRB Fermi LAT data (they over-predict the observed background). This is additional evidence that the scaling $L_\gamma - L_{\rm TIR}$ is shallower than the theoretically predicted one based on the Kennicutt-Schmidt law (i.e., that $\omega + 1 < 1.714$). However, given the sensitivity of the normalization of the scaling, $L_{\gamma,0}(\omega)$, to the number of resolved galaxies used to empirically determine its value, claiming that values of $\omega + 1 \geq 1.3$ are excluded is premature.

We note here that the spectral shape of the unresolved emission is no longer a power law for energies around 10GeV and above. The EGRB spectrum at higher energies is modified by three effects: i) because not all sources have the same special index, the hardest sources will dominate at the highest energies, giving the resulting spectrum upwards curvature (Pavlidou & Venters (2008)); ii) absorption by the extragalactic background light (EBL) will eventually become important, giving the spectrum downwards curvature (e.g., Venters, Pavlidou & Reyes (2009)); iii) electromagnetic cascades from the highest energy photons will alter the spectrum (e.g., Venters (2010)).

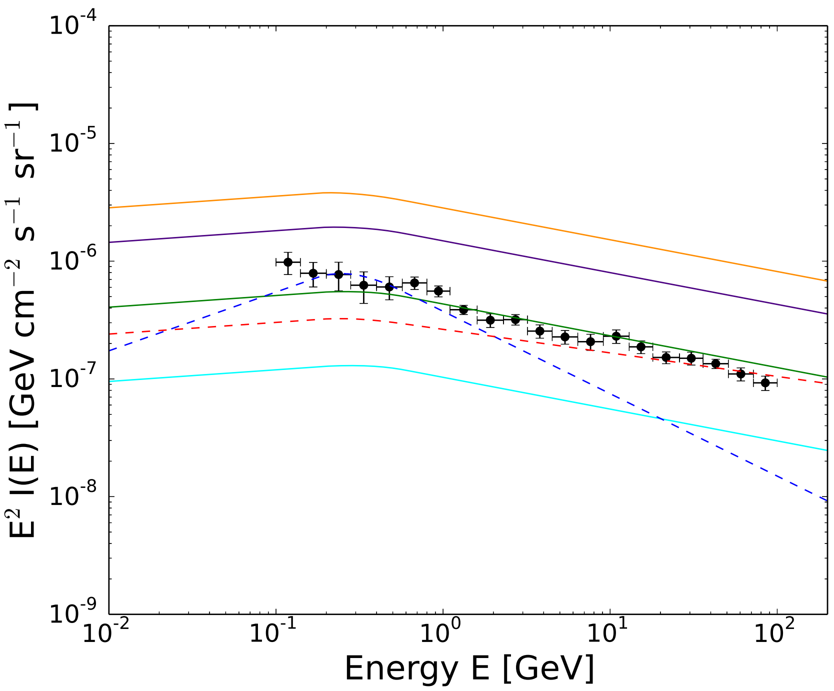

Figure 3.3: Same as Figure 3.2, but now we have also considered the starburst galaxies in our analysis. Fermi data are from (Ackermann et al. (2015)).

3.3 Normal + Starburst Galaxies

Our results, considering also the starburst galaxies in our sample, are shown in Figure 3.3. The normalization factors are obtained using all eight galaxies. Lines are the same as in Figure 3.2 and we used the same analysis to compute the contribution of normal and starburst galaxies to the EGRB for each slope. Comparing with Figure 3.2, our results are affected and especially the range of possible values of the contribution to the EGRB. The theoretical approach (indigo line) is in less tension with the empirical one (dashed red line).

The green is line is again obtained after performing least-square fitting between L_γ and $\nu L_{\rm NUV} + 2.26 L_{25\mu m}$. Our sample consists of seven galaxies, since, we exclude the Milky Way. This time the slope is equal to 1.293, i.e., $\omega + 1 = 1.293$. This is our best guess slope, since it is derived from the scaling relation between L_γ and $\nu L_{\rm NUV} + 2.26 L_{25\mu m}$. However, as discussed in §(small number statistics) the value of the empirical slope is sensitive to the small number statistics in the resolved galaxy sample, and may change when more data become available.

For normal and starburst galaxies the indigo and orange lines are still above the data, but closer. Hence, if more star-forming galaxies are resolved in gamma-rays the degree at which the EGRB is over predicted by steep $L_\gamma - L_{\mathrm{TIR}}$ scalings may change.

3.4 Effect of Star-Formation Rate

The contribution to the collective intensity from higher redshift galaxies is shown in Figure 3.4. For our model, over 50% comes from $z > 1$ and over 20% from $z > 2.5$, on average. For example, for slope 1 (cyan solid line), since we get the maximum dependence on SFR, the contribution is larger. However, in the model of Ackermann et al. (2012) (red dashed line) over 50% comes from $z > 2.1$. This is because the SFR that enters the model of Ackermann et al. (2012) is in poor agreement with the star-formation history of Hopkins & Beacom (2006). Hence, this discrepancy is due to the function $h(z)$ we introduced.

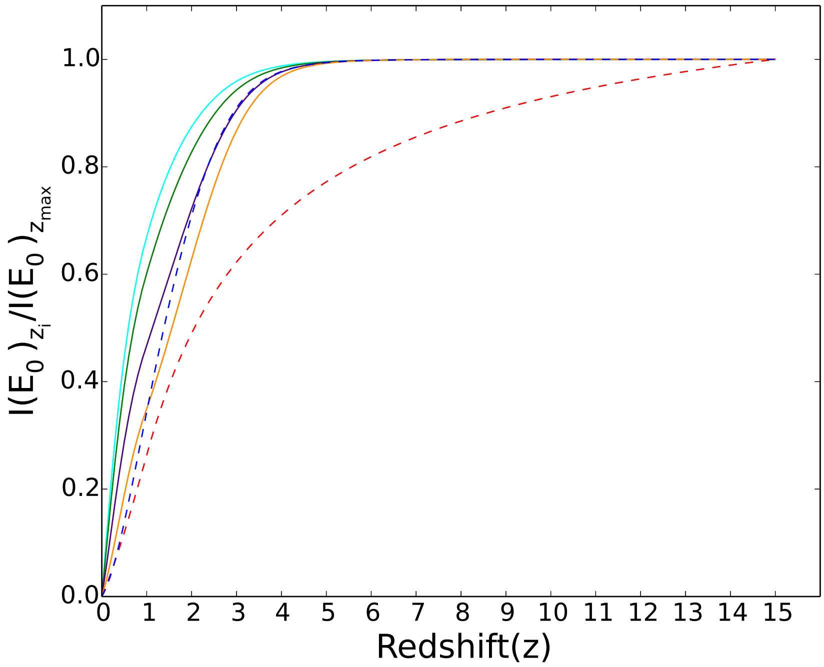

Figure 3.4: The fraction of the collective intensity of unresolved star-forming galaxies as a function of redshift. Lines represent the same assumptions as Figure 3.2.

Chapter 4

Discussion

We have estimated the contribution of unresolved star-forming galaxies to the EGRB. The model we have adopted consists of the model of Ackermann et al. (2012) and the theoretical approach of Fields et al. (2010). The first assumption of our model is that the ratio of cosmic-ray flux to SFR is constant for all normal star-forming galaxies. We also assume that losses are escape-dominated and uniform across galaxies, which probably, constitute the biggest uncertainty in our model. Future data on the EGRB and resolved galaxies will help us illustrate this assumption.

In the theoretical approach of Fields et al. (2010) it is shown that the power-law scaling between gamma-ray luminosity and SFR of a galaxy is expected to be $L_\gamma \propto \psi^{1.714}$. Thus, that is also the power-law scaling between $L_\gamma - L_{8-1000\mu m}$. However from our analysis, we conclude that the most accurate choice is a power law of 1.293 so, it seems there is a discrepancy between these two results.

However, due to the small number of the statistics such a discrepancy cannot be claimed. More resolved star-forming galaxies can affect significantly the possible contribution to the EGRB.

We consider Salpeter IMF (Salpeter (1955)) and we do not examine any dependence on the IMF. We focus on another possible parameter that can affect our results, which is the mettalicity. Considering a dependence on metallicity of the mass of stars that will undergo core-collapse supernovae (Ibeling & Heger (2013)), we have examined the effects of metallicity to our scaling relation. Hence, we assume that the supernovae rate is a function of metallicity and SFR. We have found that metallicity evolution does not affect our results. Thus, from our analysis, we conclude that this metallicity dependence is not strong enough to considerably alter the contribution of normal star-forming galaxies to the EGRB.

The peak in $E^2 dI/dE$ of each spectral shape in our Figures lies at ~ 0.3GeV because the bulk of the signal comes from z $\sim$ 1. For energies below 0.3GeV we use a spectral index of $\gamma = 1.9$ (spectral index of Milky Way) while for energies above 0.3GeV, $\gamma = 2.33$ for normal star-forming galaxies and $\gamma = 2.27$ for normal and starburst galaxies. Our model does not account for starburst galaxies and if we consider them to our sample, they affect our results. It is probable that starburst galaxies should be treated as distinct source class.

We estimated that the possible values of the normal star-forming galaxies contribution to the EGRB are between $(3-5) \times 10^{-8}$GeVcm^{-2}s^{-1}sr^{-1} and $(6-8) \times 10^{-5}$GeVcm^{-2}s^{-1}sr^{-1}. For normal and starburst galaxies the contribution is between $(9-11) \times 10^{-8}$GeVcm^{-2}s^{-1}sr^{-1} and $(2-4) \times 10^{-6}$GeVcm^{-2}s^{-1}sr^{-1}. We derive these values from two extreme scenarios of the slope of the Kennicutt-Schmidt law (Schmidt (1959); Kennicutt (1998)). We use this relation in order to relate the gas mass of a galaxy to its SFR.

Future data from the Fermi LAT are necessary in order to estimate the contribution of normal star-forming galaxies to the EGRB with less uncertainties. It is important to detect all possible components of the EGRB and distinguish their individual contribution. Especially for blazars and normal star-forming galaxies which, seem to dominate the Fermi EGRB. Extracting these two dominant sources will provide us a chance to find smaller and more exotic sources in the observed signal (Siegal-Gaskins & Pavlidou (2009)).

Bibliography

[1] Abdo, A. A., Ackermann, M., Ajello, M., et al. 2009, Physical Review Letters, 103, 251101

[2] Abdo, A. A., Ackermann, M., Ajello, M., et al. 2010, Physical Review Letters, 104, 101101

[3] Ackermann, M., Ajello, M., Allafort, A., et al. 2012, ApJ, 756, 4

[4] Ackermann, M., Ajello, M., Albert, A., et al. 2015, ApJ, 799, 86

[5] Ando, S., & Pavlidou, V. 2009, MNRAS, 400, 2122

[6] Bertone, G., Hooper, D., & Silk, J. 2005, Phys.Rept, 405, 279

[7] Buckley, J., & James, I. 1979, Biometrika, 66, 429-36

[8] Dellaert, F. 2002, Tech.Rep., Georgia Institute of Technology

[9] Dermer, C. D. 2007, The First GLAST Symposium, 921, 122

[10] Dermer, C. D., "High Energy Radiation from Black Holes", (2009), Princeton University Press

[11] Fields, B. D., Pavlidou, V., & Prodanović, T. 2010, ApJL, 722, L199

[12] Fornasa, M., & Sánchez-Conde, M. A. 2015, Phys.Rept, 598, 1

[13] Gao, Y., & Solomon, P. M. 2004, ApJ, 606, 271

[14] Hao, C.-N., Kennicutt, R. C., Johnson, B. D., et al. 2011, ApJ, 741, 124

[15] Hopkins, A. M., & Beacom, J. F. 2006, ApJ, 651, 142

[16] Ibeling, D., & Heger, A. 2013, ApJL, 765, L43

[17] Kennicutt, R. C., Jr. 1998a, ARA&A, 36, 189

[18] Kennicutt, R. C., Jr. 1998b, ApJ, 498, 541

[19] Kennicutt, R. C., & Evans, N. J. 2012, ARA&A, 50, 531

[20] Kistler, M. D., Stanek, K. Z., Kochanek, C. S., Prieto, J. L., & Thompson, T. A. 2013, ApJ, 770, 88

[21] Lacki, B. C., Thompson, T. A., Quataert, E., Loeb, A., & Waxman, E. 2011, ApJ, 734, 107

[22] Lee, J. C., Gil de Paz, A., Kennicutt, R. C., Jr., et al. 2011, ApJS, 192, 6

[23] Lequeux, J., Peimbert, M., Rayo, J. F., Serrano, A., & Torres-Peimbert, S. 1979, A&A, 80, 155

[24] Makiya, R., Totani, T., & Kobayashi, M. A. R. 2011, ApJ, 728, 158

[25] Paglione, T. A. D., Marscher, A. P., Jackson, J. M., & Bertsch, D. L. 1996, ApJ, 460, 295

[26] Pavlidou, V., & Fields, B. D. 2001, ApJ, 558, 63

[27] Pavlidou, V., & Fields, B. D. 2002, ApJL, 575, L5

[28] Pavlidou, V., & Venters, T. M. 2008, ApJ, 673, 114-118

[29] Peacock, J. A., “Cosmological Physics”, (2010), Cambridge University Press

[30] Peebles, P. J. E., “Principles of Physical Cosmology”, (1993), Princeton University Press

[31] Peng, F.-K., Wang, X.-Y., Liu, R.-Y., Tang, Q.-W., & Wang, J.-F. 2016, arXiv:1603.06355

[32] Persic, M., & Rephaeli, Y. 2010, MNRAS, 403, 1569

[33] Pohl, M. 1994, A&A, 287, 453

[34] Rodighiero, G., Vaccari, M., Franceschini, A., et al. 2010, A&A, 515, A8

[35] Rubin, V. C., Ford, W. K., Jr., & Whitmore, B. C. 1984, ApJL, 281, L21

[36] Salpeter, E. E. 1955, ApJ, 121, 161

[37] Schmidt, M. 1959, ApJ, 129, 243

[38] Siegal-Gaskins, J. M., & Pavlidou, V. 2009, Physical Review Letters, 102, 241301

[39] Skillman, E. D., Kennicutt, R. C., & Hodge, P. W. 1989, ApJ, 347, 875

[40] Stecker, F. W. 1971, NASA Special Publication, 249

[41] Stecker, F. W. 2007, Astroparticle Physics, 26, 398

[42] Stecker, F. W., & Venters, T. M. 2011, ApJ, 736, 40

[43] Tang, Q.-W., Wang, X.-Y., & Tam, P.-H. T. 2014, ApJ, 794, 26

[44] Thompson, T. A., Quataert, E., & Waxman, E. 2007, ApJ, 654, 219

[45] Torres, D. F., Reimer, O., Domingo-Santamaría, E., & Digel, S. W. 2004, ApJL, 607, L99

[46] Venters, T. M., Pavlidou, V., & Reyes, L. C. 2009, ApJ, 703, 1939

[47] Venters, T. M. 2010, ApJ, 710, 1530

[48] Weinberg, S., “Gravitation and Cosmology: Principles and Applications of the General Theory of Relativity”, (1972), John Wiley & Sons